Supplementary Figures S1-S9 for

miR-200a/b-429 downregulation is a candidate biomarker of tumor radioresistance and independent of hypoxia in locally advanced cervical cancer

Anja Nilsen[1*], Tiril Hillestad[2],Vilde E. Skingen[1], Eva-Katrine Aarnes[1], Christina S. Fjeldbo[1], Tord Hompland[1,2], Tina Sandø Evensen[2], Trond Stokke[2], Gunnar B. Kristensen[3,4], Beata Grallert[1] and Heidi Lyng [1,5*]

[1]Department of Radiation Biology, Norwegian Radium Hospital, Oslo University Hospital, Oslo, Norway. [2]Department of Core Facilities, Norwegian Radium Hospital, Oslo University Hospital, Oslo, Norway. [3]Department of Gynecological Oncology, Norwegian Radium Hospital, Oslo University Hospital, Oslo, Norway. [4]Institute of Cancer Genetics and Informatics, Oslo University Hospital, Oslo, Norway, [5]Department of Physics, University of Oslo, Oslo, Norway.

*Corresponding Authors:

Heidi Lyng, Department of Radiation Biology, Norwegian Radium Hospital, Oslo University Hospital, Pb 4950 Nydalen, Oslo 0424, Norway. Phone: 472-293-1478; E-mail: heidi.lyng@rr-research.no

Anja Nilsen, Department of Radiation Biology, Norwegian Radium Hospital, Oslo University Hospital, Pb 4950 Nydalen, Oslo 0424, Norway. Phone: 472-278-1463; E-mail: anja.nilsen@rr-research.no

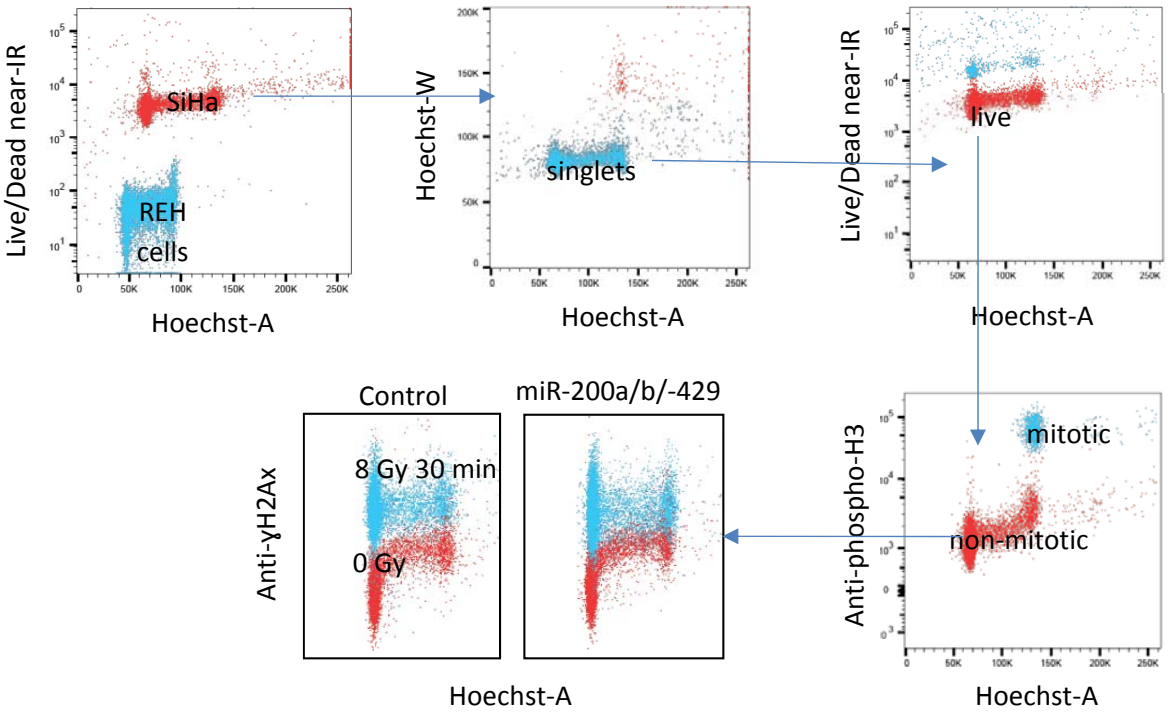

Supplementary Figure S1. **Representative example showing gating of cell subpopulations**. **Left upper panel**: SiHa cells (miR-200a/b/-429 transduced or control) and REH cells were gated on positive/negative Live/Dead near-IR staining (y-axis) and DNA content (Hoechst A, x-axis**). Middle upper panel**: Cell singlets were gated on DNA content (Hoechst-W and Hoechst-A). **Right upper panel**: Live cells were gated on Live/Dead near-IR intensity (y-axis). **Right lower panel**: Mitotic fraction was gated on anti-phospho-histone H3 intensity (y-axis) and DNA content (x-axis) and excluded from analysis of γH2Ax intensities due to high background of γH2Ax levels in mitotic cells. **Left lower panel**: The non-mitotic cell population was used in γH2Ax intensity calculations (median values).

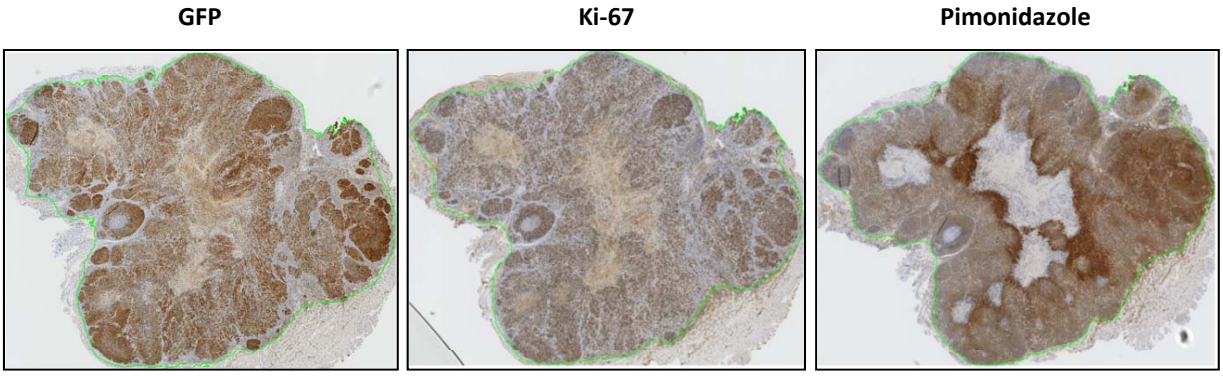

Supplementary Figure S2. IHC-staining of xenograft tumor sections. Example of IHC-stained tumor sections with anti-GFP, anti-Ki-67 and anti-pimonidazole (brown). Hematoxylin (blue) used as counterstain. ROI is marked by the green line.

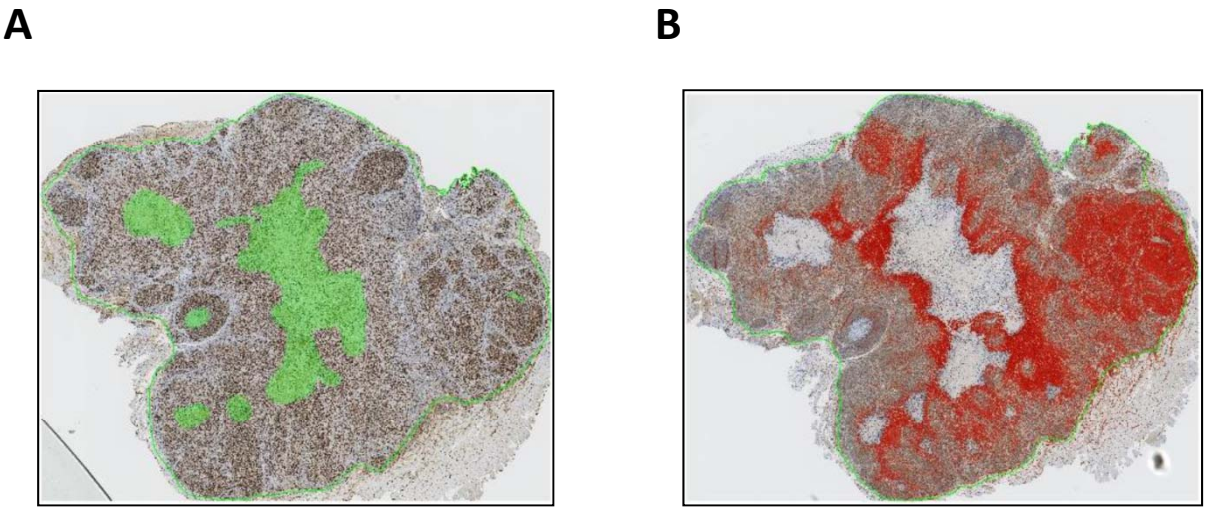

Supplementary Figure S3. **Definition of necrotic and hypoxic areas in xenograft tumor sections**. Representative RGB images of areas defined as **A**) necrotic (green) in Ki-67-stained tumor section and **B**) hypoxic (red) in pimonidazole-stained tumor section.

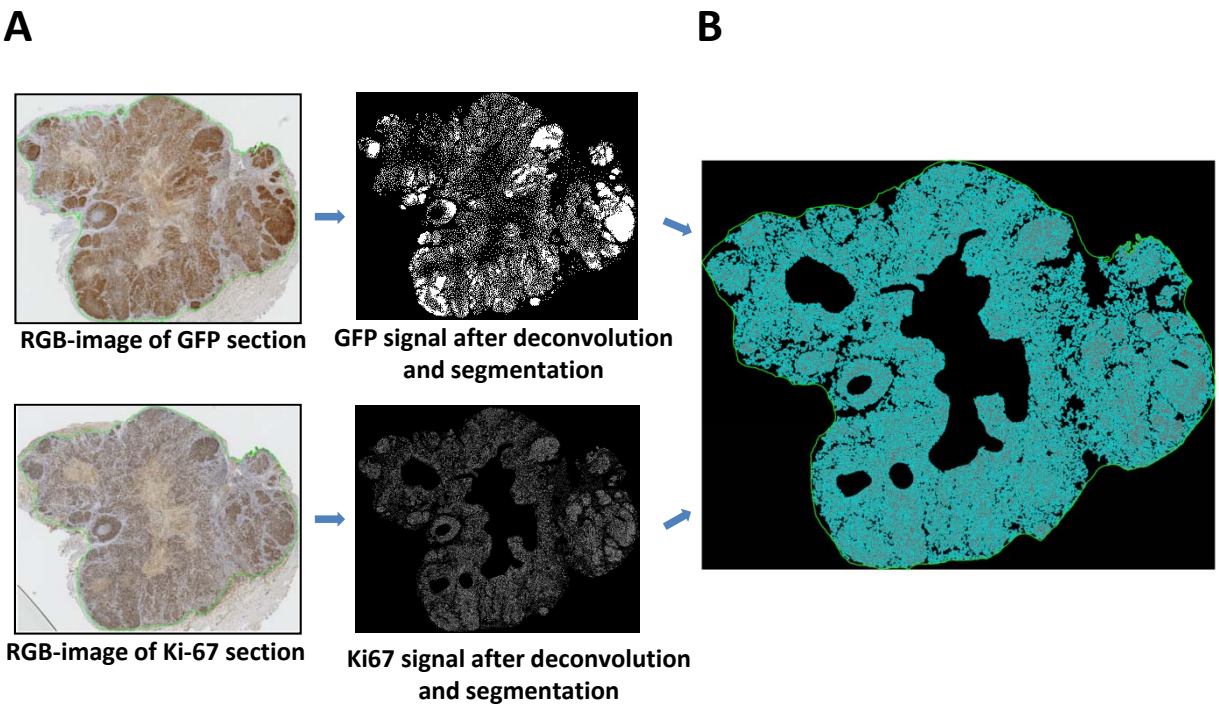

Supplementary Figure S4. **Cell segmentation**. **A**) Representative DAB and binary images of GFP-stained (upper panel) and Ki-67-stained (lower panel) tumor sections. **B**) Defined areas included after merged image processing (red: Ki-67; green: GFP).

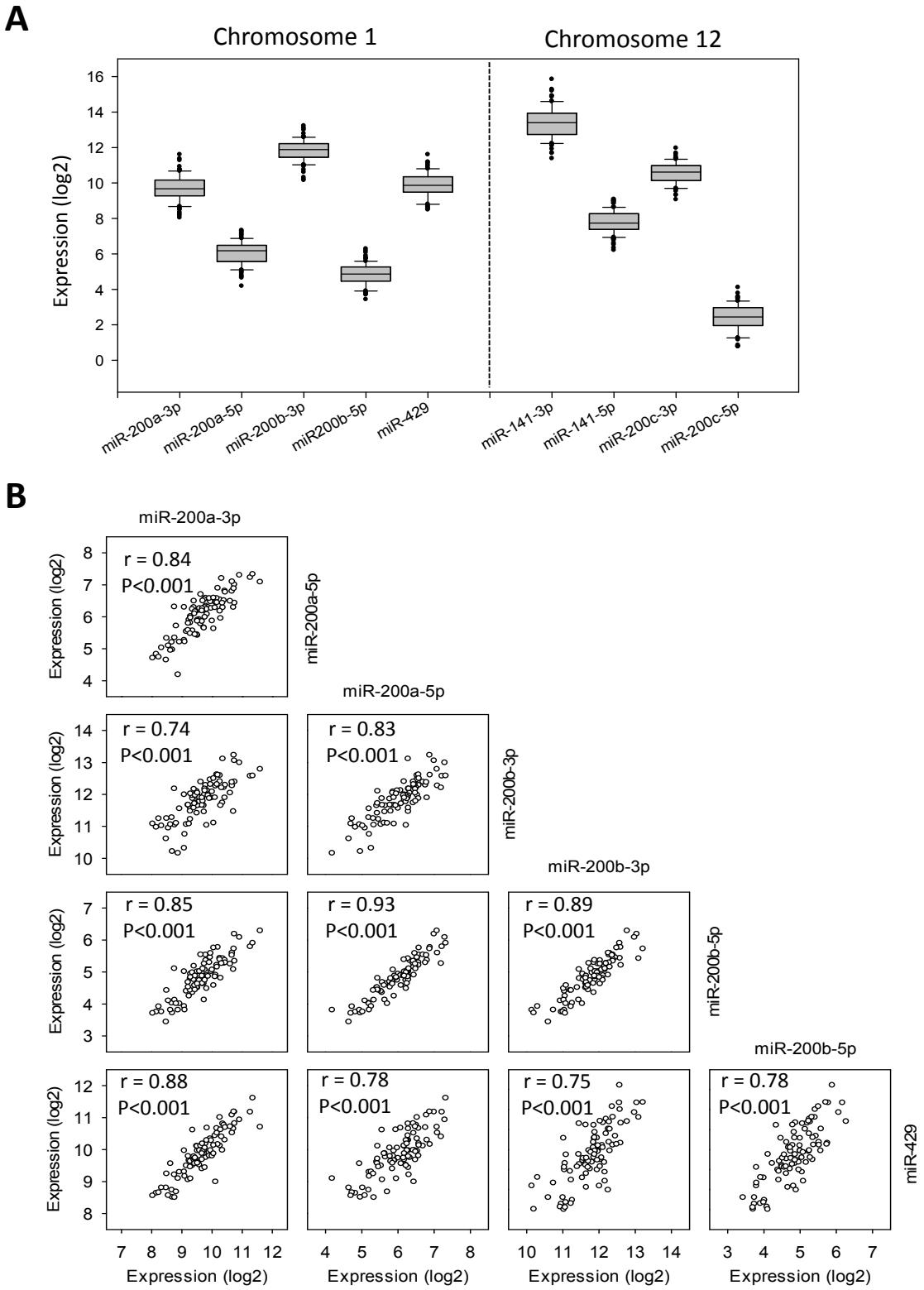

Supplementary Figure S5. **Expression of the miR-200 family in cervical cancer. A**) Expression level (RPM, $\log_2$) from small RNA sequencing data for each of the nine mature miRNAs located in miR-200 clusters on chromosome 1 (left) and chromosome 12 (right) in the explorative cohort (n=90). Box plots represent median, quartiles, range and outliers (circles). **B)**Correlations of miR-200a-5p/-3p, miR-200b-5p/-3p and miR-429 expression (RPM, log2) from small RNA sequencing data of the explorative cohort (n=90). Pearson correlation coefficients (r) and *P*-values indicated.

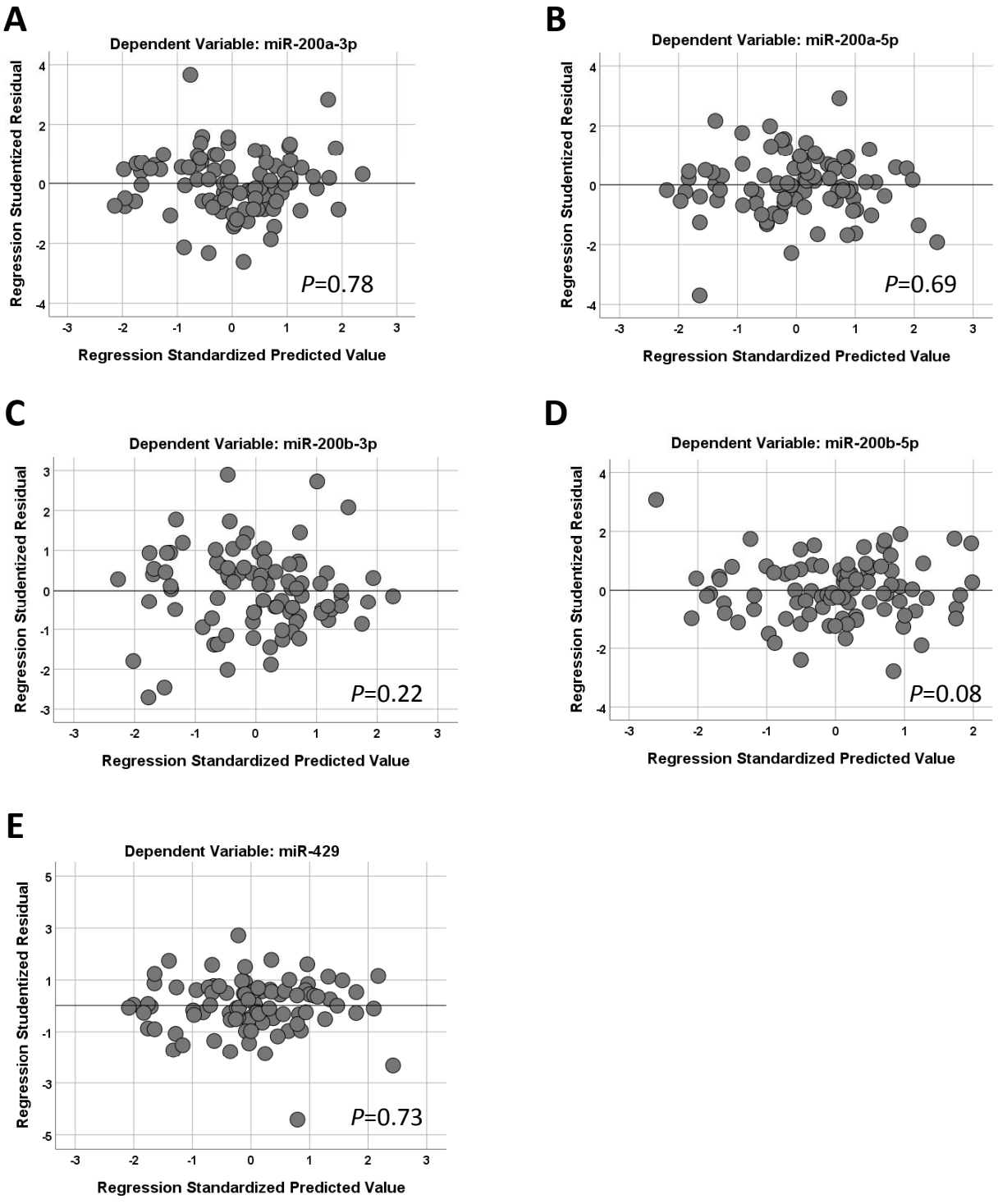

Supplementary Figure S6: Heteroscedasticity analysis. Heteroscedasticity plots of the standardized residuals of (**A)** miR-200a-3p, (**B)** miR-200a-5p, (**C)** miR-200b-3p, (**D)** miR-200b-5p and (**E)** miR-429 *versus* the predictive values of the standardized independent variables (the remaining miRNAs in the linear regression model). *P*-values from White test are indicated.

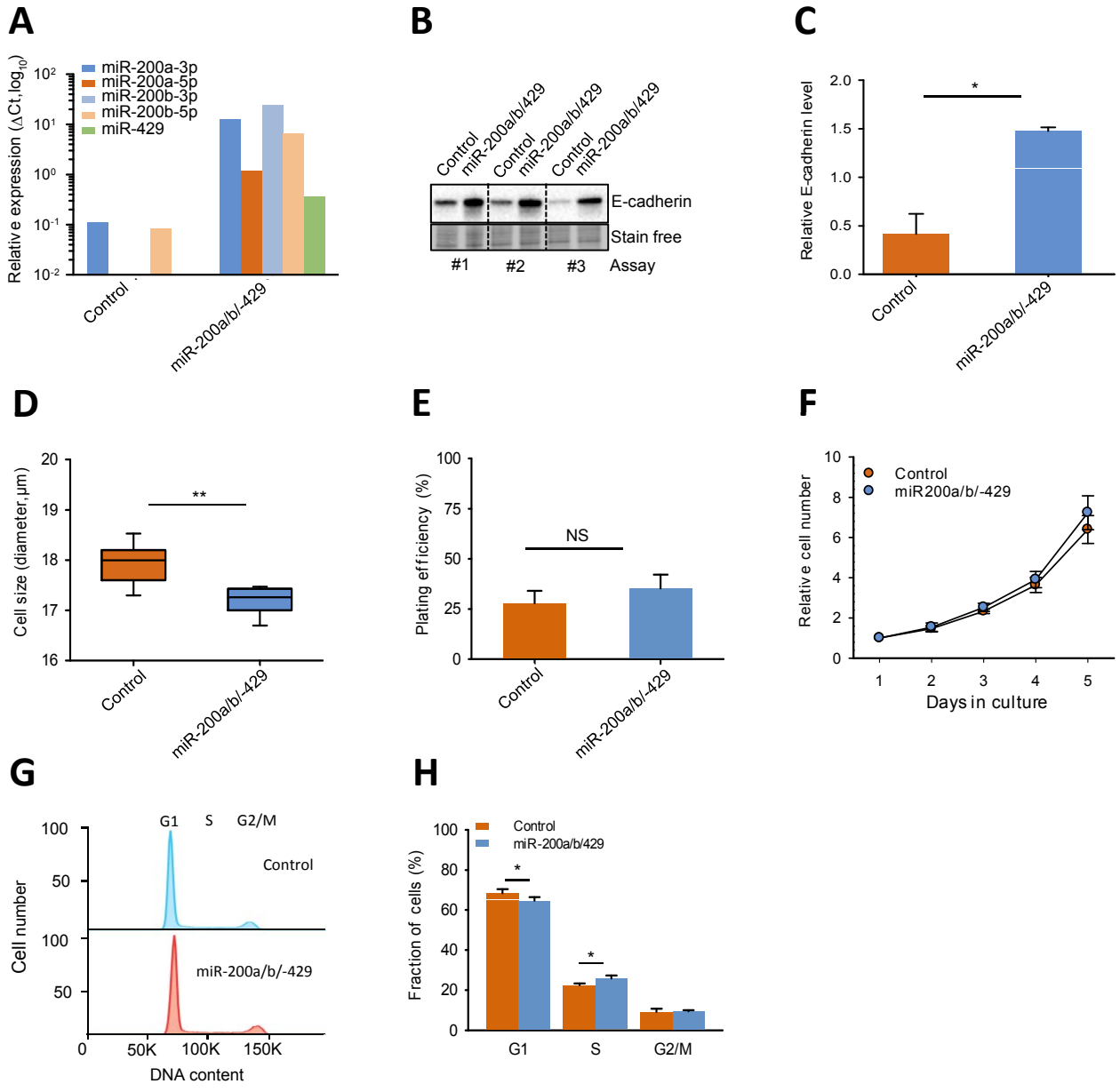

Supplementary Figure S7. *In vitro* characterization of miR-200a/b/-429-overexpressing SiHa cells. **A)** Relative expression (ΔCt) by RT-qPCR of the five mature miRNAs in the miR-200a/b-429 cluster in control cells and miR-200a/b/-429-overexpressing SiHa cells. **B)** Western blot of E-cadherin protein level of control cells and miR-200a/b/-429-overexpressing cells in total protein extracts from three independent assays. Total protein was used as loading control and detected with UV-activation of stain free blots. **C)** Quantification of E-cadherin protein level relative to total protein for the three samples shown in B (mean±SD, right). **D**) Cell diameter of control cells and miR-200a/b/-429-overexpressing cells in suspension. Box plots represent median cell diameter (µm) in samples from seven independent experiments. **E)** Quantification of plating efficiency in clonogenic assays of control cells and miR-200a/b/-429-overexpressing cells from three independent experiments (mean±SD). **F)** Relative cell number *versus* time of cultured control cells and miR-200a/b/-429-overexpressing cells. Cell number relative to number of cells at day 1 after plating in three independent assays are shown (mean±SEM). **G**) Representative histograms of DNA content and cell cycle distribution from flow cytometry analysis of control cells and miR-200a/b/-429-overexpressing cells. **H**) Fraction of control cells and miR-200a/b/-429 overexpressing cells in G_1, S and G_2/M cell cycle phase. Data from four independent experiments (mean±SEM). Students T-test or Mann-Whitney U-test; *, $P<0.05$; **, $P<0.005$.

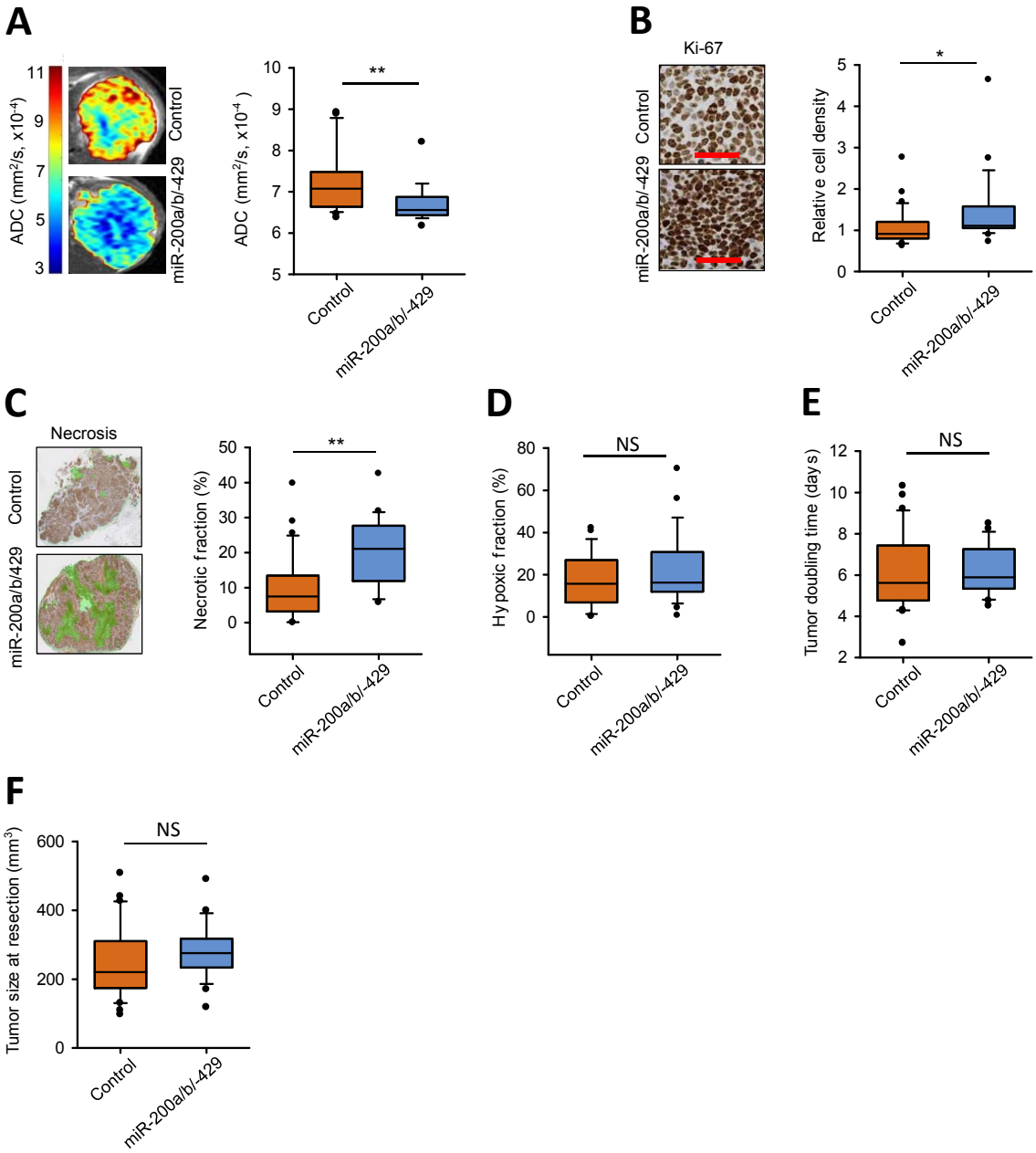

Supplementary Figure S8. *In vivo* characterization of miR-200a/b/-429-overexpressing SiHa tumors. **A**) DW-MRI assessment of cell density in control tumors and miR-200a/b/-429-overexpressing tumors. ADC maps of a representative tumor of each group with color coded scale bar of ADC-values included (left) and box plot of median ADC-values in each group (right). Non-physiological ADC-values were not included in the analysis. **B**) Cell density in control tumors and miR-200a/b/-429-overexpressing tumors. Ki-67 positive cells (brown) in representative tumor sections from each group (scale bar=60 um, left), and box plot showing number of Ki-67 positive cells relative to GFP-positive parenchyma region in co-registered tumor sections (right). **C)** Necrosis in control tumors and miR-200a/b/-429-overexpressing tumors. Necrotic regions (green) in representative tumor sections from each group (left), and box plot of necrotic fraction relative to the entire tumor region (right). **D**) Hypoxic fraction in control tumors and miR-200a/b/-429 overexpressing tumors. Box plot of pimonidazole-positive fraction relative to the entire tumor region. Necrotic regions defined in co-registered tumor sections were excluded from analysis. **E**) Tumor doubling time (days) and **F**) tumor volume at resection in control and miR-200a/b/-429-overexpressing tumors assessed by T_2W-MRI. A-F), Box plots represent median, quartiles, range and outliers (circles); Students T-test or Mann-Whitney U-test statistics, $^{**}P < 0.005$ NS, not significant; n=30 control tumors; n=23 miR-200a/b/-429-overexpressing tumors.

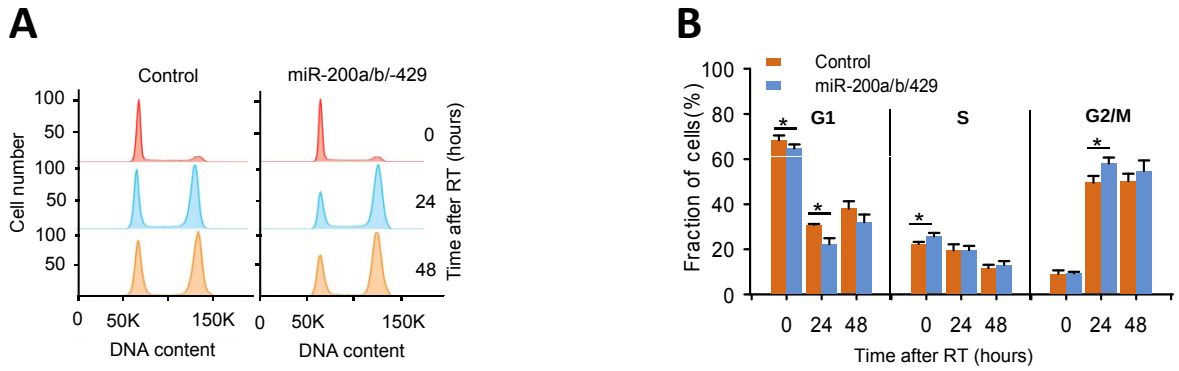

Supplementary Figure S9. Radiation effect on cell cycle distribution in miR-200a/b/-429-overexpressing SiHa cells. **A**) Representative histograms of DNA content and cell cycle distribution from flow cytometry assays of control cells and miR-200a/b/-429-overexpressing cells analyzed before (0 hours) and at indicated timepoints after exposure to 8 Gy. **B)** Fraction of control cells and miR-200a/b/-429 overexpressing cells in G_1, S and G_2/M cell cycle phase analyzed before (0 hours) and at indicated timepoints after exposure to 8 Gy. Data from four independent experiments (mean±SEM). Students T-test; *, $P<0.05$.